TU Delft

Delft University of Technology

Document Version
Final published version

Licence
Dutch Copyright Act (Article 25fa)

Citation (APA)
Abdelwahab, A. N. M. K., Farmani, Z., Kuipers, H., Tichem, M., Fan, J., & Zhang, K. (2026). Liquid-Assisted Contactless Adhesive Bonding: Experimental validation and 2D Multiphysics simulation. In *Proceedings of the 2026 27th International Conference on Thermal, Mechanical and Multi-Physics Simulation and Experiments in Microelectronics and Microsystems (EuroSimE)* (International Conference on Thermal, Mechanical and Multi-physics Simulation and Experiments in Microelectronics and Microsystems :). IEEE. https://doi.org/10.1109/EuroSimE69483.2026.11511664

Important note
To cite this publication, please use the final published version (if applicable).
Please check the document version above.

Copyright
In case the licence states “Dutch Copyright Act (Article 25fa)”, this publication was made available Green Open Access via the TU Delft Institutional Repository pursuant to Dutch Copyright Act (Article 25fa, the Taverne amendment). This provision does not affect copyright ownership.
Unless copyright is transferred by contract or statute, it remains with the copyright holder.

Sharing and reuse
Other than for strictly personal use, it is not permitted to download, forward or distribute the text or part of it, without the consent of the author(s) and/or copyright holder(s), unless the work is under an open content license such as Creative Commons.

Takedown policy
Please contact us and provide details if you believe this document breaches copyrights.
We will remove access to the work immediately and investigate your claim.

This work is downloaded from Delft University of Technology.

2026 27th International Conference on Thermal, Mechanical and Multi-Physics Simulation and Experiments in Microelectronics and Microsystems (EuroSimE) | 979-8-3315-6249-6/26/$31.00 ©2026 IEEE | DOI: 10.1109/EuroSimE69483.2026.11511664

Liquid-Assisted Contactless Adhesive Bonding: Experimental validation and 2D Multiphysics simulation

Ahmed Abdelwahab
ECTM
Delft University of Technology
Delft, The Netherlands
a.n.m.k.abdelwahab@tudelft.nl

Zohreh Farmani
PME
Delft University of Technology
Delft, The Netherlands
Z.Farmani@tudelft.nl

Hans Kuipers
ITEC Equipment
Nijmegen, The Netherlands
j.j.kuipers@itecequipment.com

Marcel Tichem
PME
Delft University of Technology
Delft, The Netherlands
M.Tichem@tudelft.nl

Jiajie Fan
ECTM
Delft University of Technology
Delft, The Netherlands
J.Fan-3@tudelft.nl

G. Q. Zhang
ECTM
Delft University of Technology
Delft, The Netherlands
G.Q.Zhang@tudelft.nl

***Abstract*— Handling ultra-thin semiconductor dies during assembly remains challenging due to their mechanical fragility and sensitivity to placement forces. Contactless die transfer methods reduce mechanical loading and have potential to enable higher placement speeds and improved throughput but introduce challenges such as uncontrolled impact dynamics, die rebound, and misalignment during landing. This work investigates a liquid-assisted contactless adhesive bonding approach in which droplets deposited on stencil-printed conductive adhesive act as transient damping and alignment media during die landing. Dummy silicon dies with a gold (Au) surface finish were released from a short distance onto the adhesive. Four liquids with different physical and chemical properties—deionized (DI) water, isopropyl alcohol (IPA), acetone, and liquid flux—were investigated to evaluate the influence of key fluid parameters, including surface tension, viscosity, and density, on die impact dynamics, stabilization, and subsequent bonding quality. The results demonstrate that droplet material properties significantly influence die landing dynamics in liquid-assisted contactless assembly. Among the investigated liquids, deionized water enabled reliable die entrapment and damping. In contrast, for the lower-surface-tension solvents isopropyl alcohol (IPA) and acetone, the droplets were not sufficiently confined under the experimental conditions, and therefore no direct die entrapment was observed, although impact damping was still achieved. Die entrapment and stabilization behavior were analyzed using high-speed camera recordings and complementary two-dimensional simulations performed in COMSOL Multiphysics. Furthermore, the impact of the droplets on the resulting bond interface and joint quality was evaluated through post-bond characterization. The study provides insight into droplet-mediated die landing and offers guidelines for selecting liquids for reliable contactless micro-assembly.**

Keywords*— *Liquid-assisted, Self-alignment, Adhesive bonding, Pick-and-Place, Pick-and-Release, COMSOL

I. Introduction

The continuous scaling of semiconductor devices and the adoption of heterogeneous and vertically stacked integration architectures have increased package density while significantly reducing die thickness[1]. Although these advances enable compact and high-performance systems, ultra-thin dies become mechanically fragile and highly susceptible to cracking, chipping, and warpage during handling and assembly[2].

Defects and micro-cracks generated during wafer thinning and sawing can further propagate under assembly stresses, making die placement and bonding critical challenges in advanced semiconductor packaging[3].

Conventional die bonding relies on mechanical pick-and-place systems that apply placement forces of approximately 0.2–1 N.[4] which can damage ultra-thin dies, especially in high-throughput applications such as micro-LED manufacturing. Contactless transfer methods, including laser die transfer and acoustic levitation, have been proposed to reduce mechanical loading, but they introduce challenges such as uncontrolled impact dynamics, die rebound, and lateral misalignment.

Adhesive-based interconnect technologies provide an alternative to traditional solder bonding, enabling low-temperature processing, compatibility with sensitive substrates, and fine-pitch interconnections [5]. Conductive and anisotropic adhesives also provide mechanical attachment and electrical interconnection through conductive fillers in polymer matrices, making them suitable for applications where conventional soldering is limited [5-7].

However, adhesive bonding alone does not resolve challenges associated with contactless die landing, particularly rebound and misalignment. Capillary self-alignment (CSA) has therefore emerged as an effective strategy for precise microchip placement in advanced packaging and micro-assembly systems[8-10]. Driven by surface energy minimization, liquid-mediated alignment provides a passive self-correcting mechanism that compensates for placement errors without active control[11]. When a solid component interacts with a liquid interface, interfacial forces drive the system toward an equilibrium configuration, enabling accurate alignment when the characteristic meniscus size is smaller than the capillary length and surface tension dominates gravitational forces.[12]

In this work, a liquid-assisted contactless adhesive bonding method is proposed, where droplets pre-dispensed on an substrate coated with adhesive act as transient damping and alignment media during die landing. Upon impact, droplets dissipate kinetic energy, suppress rebound, and induce capillary forces that drive passive self-alignment of the die. Experimental validation combined with two-dimensional Multiphysics simulations provides insight into the coupled fluid–structure interactions governing impact damping, droplet deformation, and capillary-driven

979-8-3315-6249-6/26/$31.00 ©2026 IEEE Authorized licensed use limited to: TU Delft Library. Downloaded on June 15,2026 at 10:18:25 UTC from IEEE Xplore. Restrictions apply.

alignment, demonstrating the potential of this approach for next-generation semiconductor packaging and micro-assembly applications.

II. Liquid-Assisted Concept

In the dry drop attach process, dies are picked using a vacuum pick-up tool and optically aligned above a substrate on which a conductive adhesive is stencil printed. The dies are then positioned approximately 1 mm above the adhesive layer and released, allowing them to fall onto the substrate.

Under ideal conditions, where the adhesive layer is flat, uniform, and defect-free, the dies can land safely. However, safe landing requires the dies to fall parallel to the substrate surface. In practice, this condition is often not achieved. A significant fraction of the dies exhibit tilting upon release, resulting in rotational motion during the fall. Although the drop height is relatively small and limits full rotation, some dies still land on one of their edges. In certain cases, this causes the dies to rebound away from the adhesive layer, while in other cases the dies land with misalignment that cannot be corrected later in the process.

To mitigate these issues, a liquid-assisted die attach approach is proposed. In this method, a small droplet provides impact damping by absorbing part of the die's kinetic energy during landing. Ideally, the droplet also enables die entrapment and self-alignment, thereby improving placement robustness and alignment accuracy.

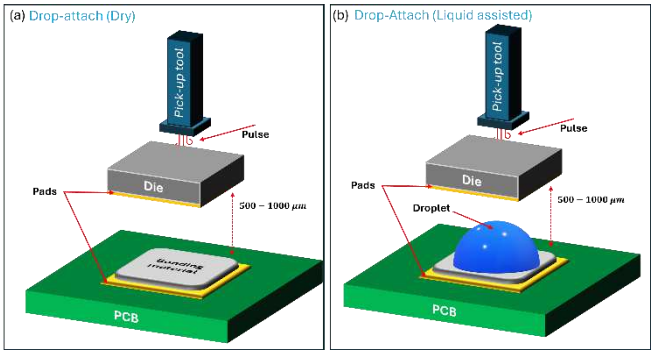


Fig. 1 Sketch of the die attach processes studied in this work. (a)Drop-attach , (b) the proposed liquid-assisted Drop- Attach.

Fig.1 shows the main difference between the dry drop attach and the liquid-assisted method.

III. Materials and Methods

A. Substrates and Dies Fabrication

A printed circuit board (PCB) was designed featuring arrays of 2 mm × 2 mm bond pads, matching the dimensions of the dummy dies. The PCBs were fabricated with an electroless nickel immersion gold (ENIG) surface finish to ensure corrosion resistance, reliable electrical connectivity, and compatibility with the conductive adhesive used in this study.

Dummy dies with a gold (Au) surface finish were fabricated from 4-inch, single-side-polished silicon wafers with a thickness of 525 µm. First, a 300 nm SiO_2 layer was grown on the wafers by wet thermal oxidation. Subsequently, a 10 nm chromium (Cr) adhesion layer was deposited by evaporation, followed by a 200 nm Au evaporated layer to form the top metallization. After completing the fabrication and metallization processes, the wafers were diced to be 1.92mmx1.92mm using a wafer saw (Disco DAD321) equipped with an S2040 dicing blade. Fig. 2(a) illustrates the PCB layout, 2(b) presents a cross-sectional view of the PCB, and 2(c) shows a cross-sectional schematic of the fabricated dummy dies.

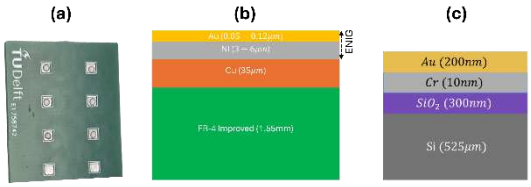


Fig. 2 (a) PCB with added droplets, (b) sketch of the PCB cross-section, (c) Cross-sectional sketch of the dummy dies (not to scale)

B. Bonding Material and Stencil Printing

A commercially available conductive adhesive was selected for the die-attach process. The formulation contains approximately 80 wt.% silver particles dispersed within an acrylate-based polymer resin, which cures to form the structural binder. The adhesive was processed using a snap-cure profile consisting of 60 s at 185 °C on a hot plate. Adhesive deposition was performed using a 100 µm-thick laser-cut stainless-steel stencil in combination with a manual eC-Stencil-Mate system (Eurocircuits), enabling controlled transfer of adhesive onto the metal pads patterned on the substrate. Minor non-uniformities in the printed adhesive patterns were observed, particularly near the edges, which can arise from process-related variations inherent to manual stencil printing operations[13].

C. Droplet materials and Dispensing

Four liquid materials were selected for droplet-based testing. Deionized (DI) water was employed as a reference material. Two commonly used solvents with lower surface tension than water, acetone and isopropyl alcohol (IPA), were chosen due to their high compatibility with adhesives and their potential use as adhesive diluents. In addition, a semiconductor-industry-compatible liquid flux with higher surface tension than water was included to enable assessment of die entrapment and to investigate the influence of surface tension on the process window, defined in terms of release distance and die velocity.

Two dispensing methods were employed for droplet generation. Deionized (DI) water was dispensed using a droplet generator to ensure controlled and repeatable droplet formation. To prevent contamination and clogging of the droplet generator, it was exclusively used with DI water. All other liquid materials were dispensed using a manual laboratory micropipette with a dispensing range of 0.1–2.5 µL. To maintain consistency across all experiments, a droplet volume of 0.1 µL was used in all cases, regardless of the dispensing method.

The PCB used in this study did not incorporate intentionally fabricated geometrical confinement features, such as pedestals or recessed pockets, for liquid confinement. Four liquids were investigated: deionized (DI) water, liquid flux, isopropyl alcohol (IPA), and acetone. Distinct differences in wetting behavior were observed among these liquids on the printed adhesive surface.

Authorized licensed use limited to: TU Delft Library. Downloaded on June 15,2026 at 10:18:25 UTC from IEEE Xplore. Restrictions apply.

DI water and liquid flux maintained a more defined droplet shape after dispensing due to their relatively higher surface tension and reduced tendency to spread. However, the confinement of these droplets was strongly influenced by the characteristics of the printed adhesive pattern produced during the stencil printing process.

Following stencil printing, the printed adhesive pattern exhibited noticeable imperfections, particularly near the edges, as described in Section B. These imperfections were characterized by locally increased adhesive thickness along the perimeter of the printed area. This edge thickening is attributed to the stencil separation process. During stencil lift-off, residual adhesion between the adhesive and the stencil mask can cause deformation of the printed pattern as the stencil is separated from the substrate. As a result, excess adhesive tends to accumulate near the edges of the printed feature.

Interestingly, these edge-related adhesive accumulations effectively formed sidewall-like structures surrounding the printed adhesive region. The resulting topography created a shallow cup-like geometry around the adhesive area. Although these features were not intentionally designed as confinement structures, they provided localized liquid containment. Under these conditions, small droplets of DI water and liquid flux could be reliably confined within the printed adhesive region without overflowing the boundaries.

In contrast, IPA and acetone, both characterized by relatively low surface tension, did not form stable droplets upon deposition. Instead, manual pipetting resulted in rapid spreading of the liquid over the adhesive surface, producing a thin liquid film. Even in the presence of the shallow cup-like structures formed by the edge thickening, these liquids did not remain localized within the printed adhesive region and instead spread across the surface. Due to the absence of a well-defined droplet and the lack of effective lateral confinement, die entrapment and subsequent self-alignment were not achieved when these liquids were used.

Nevertheless, the presence of this thin liquid layer provided effective damping during the impact of the die with the adhesive paste. The liquid film acted as a cushioning medium that dissipated part of the kinetic energy during impact, thereby significantly reducing impact forces and enabling a near-perfect transfer success rate.

Fig. 6 shows a 3D microscope scan of the stencil-printed adhesive on a 2 mm × 2 mm pad, revealing pronounced edge thickening. The adhesive height near the pad perimeter is at least 10 µm greater than that of the central region. Although the nominal pad dimensions were 2 mm × 2 mm, the flat central region of the printed adhesive remained sufficiently large to ensure full contact with the die. Due to kerf loss during dicing, the actual die dimensions were approximately 1920 µm × 1920 µm, while the flat adhesive area was at least 1950 µm × 1950 µm. Consequently, complete die–adhesive contact was achieved, while the peripheral adhesive thickening simultaneously contributed to liquid confinement.

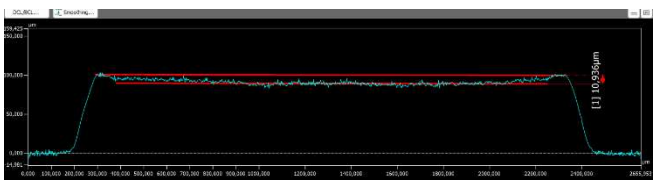


Fig. 3 3D-scan showing 10 microns height difference between the Centre and the edges of the stencil printed adhesive.

D. Die Attachment

The experiments were conducted using two separate systems: a Tresky T-3000-PRO semi-automatic die bonder and a custom-built setup integrating a high-speed camera. During the air-drop tests, dies were picked up using a vacuum gripper, optically aligned above the substrate, and released from a height of 1mm above the adhesive layer deposited on the substrate. Die release was initiated by an air pulse of 0.15 bar applied for a duration of 100 ms. For both systems the drying and curing were conducted using a hot plate.

E. Drying

The drying process was identified as a critical step in the proposed approach, as it ensures complete evaporation of the liquid droplet before the adhesive reaches its curing temperature. If curing occurs while liquid remains trapped at the die–adhesive interface, effective bond formation cannot be achieved. To investigate this behavior, reference experiments were conducted by directly heating the substrates to 180 °C, the adhesive curing temperature, without a temperature ramp or intermediate drying step.

Under these conditions, samples assembled with deionized (DI) water exhibited pronounced failures. Rapid evaporation of trapped water generated gas bubbles at the interface, producing a popcorn-like failure in which the die was displaced or ejected from the adhesive layer, sometimes moving out of the camera's field of view. Although similar behavior could theoretically occur with acetone or isopropyl alcohol (IPA), no such failures were observed. This is attributed to the dwell time between solvent dispensing, alignment, die release, and heating (several seconds to 2–3 minutes), which allowed partial evaporation of these more volatile solvents and reduced the amount of trapped liquid. In contrast, liquid flux evaporated more slowly, resulting in a gradual and stable drying process.

Based on these observations, the curing protocol was adjusted for each droplet material to allow controlled evaporation at lower temperatures prior to curing, ensuring complete droplet removal and preventing the observed failures.

Table 1 Optimized drying and curing parameters for different droplets

Droplet	Drying and Curing parameters
Dry	60s @185℃
DI water	180s @70℃+60s @100+60s @185℃
IPA	120s @50℃+60s @185℃
Acetone	120s @50℃+60s @185℃
Liquid Flux	120s @80℃+90s @130℃+60s @185℃

F. Die Entrapment: Numerical Simulations and Experimental validation

The Two-dimensional (2D) simulations were conducted using COMSOL Multiphysics to investigate the dynamics of chip entrapment at a liquid interface. The model geometry replicated the experimental setup, consisting of a silicon chip (2 × 0.5 mm²), a PCB pad (2 × 0.1 mm²), a fixed chip-droplet distance of 1 mm, and a water droplet of volume 100 nL. To capture droplet spreading and its

Authorized licensed use limited to: TU Delft Library. Downloaded on June 15,2026 at 10:18:25 UTC from IEEE Xplore. Restrictions apply.

interaction with the chip, three physics interfaces were coupled: a Laminar Flow model solving the Navier–Stokes equations, a Phase Field model tracking the air–water interface, and a Solid Mechanics model describing chip motion and fluid–structure interaction. This coupled approach allows droplet deformation, wetting, and chip movement to be resolved in time. Surface tension, viscosity, and gravity were included using experimentally measured material parameters.

The experimental setup used for the chip entrapment experiments, consisting of a chip pick-and-place system and a high-speed imaging system. The chip is manipulated using a vacuum gripper. The entire process—including chip release, droplet-mediated entrapment, and final chip alignment—is recorded using a Photron S6 high-speed camera.

The simulations aimed to capture the key physical mechanisms governing capillary-driven chip entrapment while systematically varying fluid types. The primary goal is to understand how the fluid properties affect droplet spreading, chip alignment, and entrapment efficiency. Optimizing these properties can improve the speed and stability of droplet-mediated chip assembly.

We investigated the differences in behavior among four fluids: DI water (γ = 0.072 N/m, μ = 0.001 Pa·s), Acetone (γ = 0.025 N/m, μ = 0.00032 Pa·s), IPA (γ = 0.023 N/m, μ = 0.002 Pa·s), Liquid flux (γ = 0.04 N/m, μ = 0.01 Pa·s). Figure 13 shows snapshots from the experiments versus 2D simulations for DI water at different times. In the experimental images (a), the droplet initially forms a nearly spherical cap upon deposition due to surface tension dominance. As time progresses, the droplet spreads over the adhesive layer, increasing its contact radius while reducing its height. This behavior is governed by the balance between surface tension, viscous forces, and adhesive interactions with the substrate.

The 2D simulation results shown in (b) reproduce the general spreading trend observed in the experiments. The simulated droplet profile captures the gradual reduction in contact angle and the increase in wetting area over time. The agreement between the experimental observations and the numerical results suggests that the simulation model reasonably represents the wetting and spreading physics of DI water on the adhesive layer. Minor differences between the two may arise from simplifications in the 2D model, uncertainties in surface properties.

Fig. 4 shows high-speed camera images together with simulation results, illustrating the predicted droplet shape and spreading dynamics at comparable time instances. While Figure 5 illustrates the dynamic spreading and capillary-driven alignment behavior of three different liquids—acetone, IPA, and liquid flux—on an adhesive layer. The differences in spreading rate and final alignment time are primarily governed by the surface tension (γ) and viscosity (μ) of the fluids.

In acetone (a), the droplet spreads rapidly after deposition. Acetone has very low viscosity (~0.00032 Pa·s) and relatively low surface tension (~0.025 N/m), which allows the liquid to flow easily and redistribute quickly across the adhesive layer.

The low viscous resistance enables fast interface motion, resulting in rapid wetting and shorter alignment time. The droplet quickly forms a thin liquid film between the surfaces and reaches its equilibrium configuration earlier compared with the other fluids.

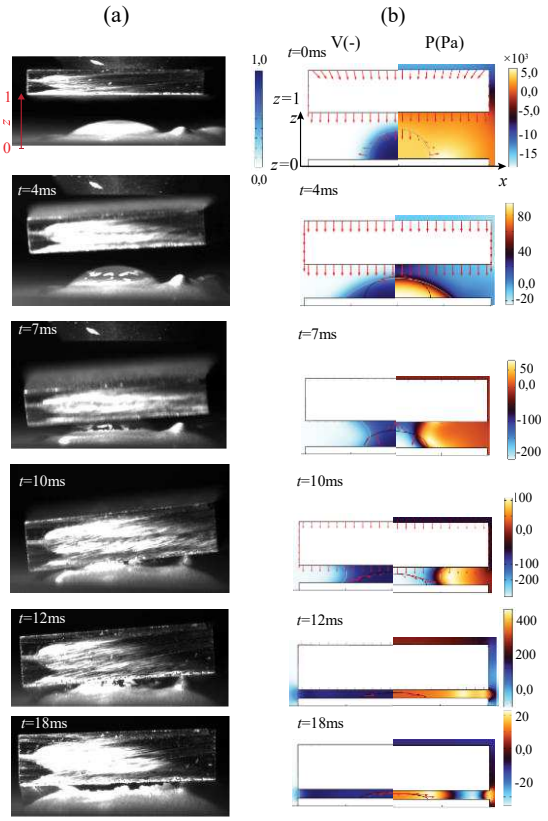


Figure 4 Time evolution of a DI water droplet deposited on an adhesive layer. (a) Experimental images showing the spreading behavior of the droplet at different times after deposition. (b) Corresponding 2D numerical simulation.

In acetone (a), the droplet spreads rapidly after deposition. Acetone has very low viscosity (~0.00032 Pa·s) and relatively low surface tension (~0.025 N/m), which allows the liquid to flow easily and redistribute quickly across the adhesive layer. The low viscous resistance enables fast interface motion, resulting in rapid wetting and shorter alignment time. The droplet quickly forms a thin liquid film between the surfaces and reaches its equilibrium configuration earlier compared with the other fluids.

For IPA (b), the spreading process is slightly slower. Although IPA has a similar surface tension (~0.023 N/m) to acetone, its viscosity (~0.002 Pa·s) is higher. This increased viscous resistance slows down the internal flow within the droplet and reduces the rate of spreading. As a result, the liquid front advances more gradually and the time required to achieve final alignment is longer than that observed for acetone.

In the case of liquid flux (c), the spreading process is significantly slower and more controlled. Liquid flux typically exhibits higher viscosity (~0.01 Pa·s) and higher surface tension (~0.04 N/m) compared with acetone and IPA. The increased viscosity strongly resists fluid motion, limiting the rate at which the liquid redistributes across the interface. At the same time, the higher surface tension promotes stronger capillary forces that help maintain the droplet shape and influence the alignment process. Consequently, the droplet spreads more gradually and the

Authorized licensed use limited to: TU Delft Library. Downloaded on June 15,2026 at 10:18:25 UTC from IEEE Xplore. Restrictions apply.

final alignment occurs at a later time compared with the lower-viscosity fluids.

The results demonstrate that viscosity primarily controls the rate of spreading and alignment, while surface tension governs the capillary forces driving the interface shape and wetting behavior. Fluids with lower viscosity spread faster and achieve alignment more quickly, whereas higher-viscosity fluids exhibit slower spreading dynamics and longer stabilization times.

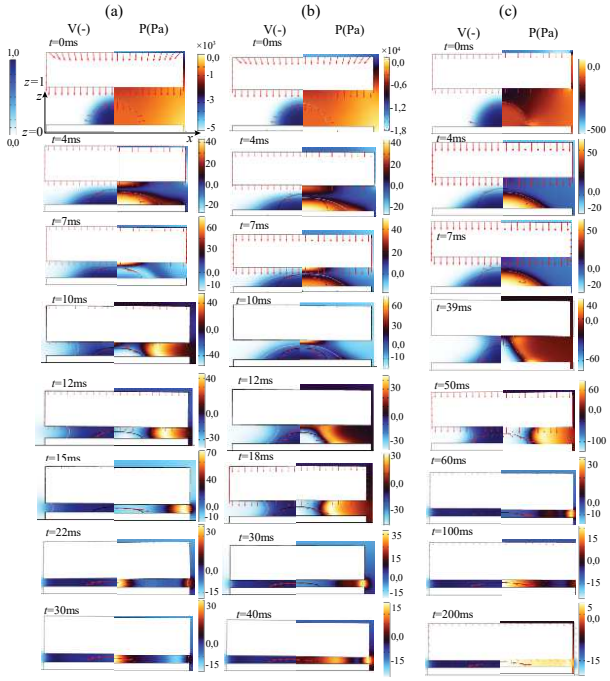


Fig. 5 Time evolution of droplet spreading and alignment on an adhesive layer for different liquids obtained from 2D simulations. The columns represent different fluids: (a) Acetone, (b) IPA, and (c) Liquid flux.

This behavior indicates that stronger surface tension generates larger capillary pressure gradients, which accelerate the spreading of the droplet beneath the chip and enhance the capillary forces responsible for chip alignment and entrapment. In contrast, at low surface tension values, the capillary driving force is weaker, resulting in slower spreading and delayed chip alignment. The droplet takes longer to fill the gap between the chip and the substrate, leading to longer equilibration times.

The simulation snapshots also show that under these conditions the droplet interface spreads more gradually and the alignment dynamics is unstable with the final tilted position.

The results demonstrate that surface tension is a dominant parameter controlling the speed of capillary-driven chip entrapment. Higher surface tension fluids generate stronger capillary forces and faster pressure-driven flow beneath the chip, leading to shorter equilibration times and more rapid chip alignment. However, when $\gamma \geq 0.1$ N/m the equilibrium time becomes independent from the surface tension. These findings suggest that selecting fluids with sufficiently high surface tension while maintaining manageable viscosity can significantly improve the efficiency of droplet-assisted chip assembly.

IV. Characterization

A. Adhesive Profile and Volume

To evaluate potential defects arising from manual stencil printing and curing-related effects, such as shrinkage or void formation, a series of control experiments was conducted without die attachment. These tests focused on quantifying the printed adhesive volume and average layer thickness, as well as verifying that the manual stencil-printing process produced a flat and uniform adhesive layer. Following inspection, a limited number of PCBs were rejected due to irregularities in the adhesive profile, primarily associated with the formation of elevated adhesive regions at the pad edges, rendering them unsuitable for the proposed drop-attach method.

The adhesive volume was measured before and after curing using a 3D confocal laser scanning microscope (Keyence VK-250). In addition to volumetric analysis, the average adhesive layer thickness was extracted from the acquired 3D surface profiles. A theoretical adhesive volume was calculated by assuming a uniform, flat adhesive layer fully covering the pad area, modeled as a thin film or rectangular cuboid. Comparison between this theoretical volume and the experimentally measured volume revealed that the printed adhesive consistently exhibited a smaller volume than predicted by the idealized model. The average adhesive thickness was measured to be 91.22 ± 1.56 µm prior to curing and 66.17 ± 1.45 µm after curing.

A summary of the adhesive volume measurements before and after curing is presented in Table 1, highlighting the changes induced by the curing process.

Table 2 Adhesive volume through different process stages(dry case)

Pad size (mm)	Theoretical printed volume (μL)	Volume as printed (μL)	Volume after curing (μL)	Actual reduction %
2.00x2.00	0.3649	0.3450	0.2699	21.77

To identify and better understand the droplet effect on the adhesive and to ensure the complete evaporation of the droplets, we measured the final cured volume of adhesive were droplets were dispensed on.

In case of IPA and acetone the volume of the adhesive remained similar to the dry case however the 3d-scans showed some changes in terms of the profile as if the center area was etched away and the edges area were getting higher this is most likely to the interaction between the droplets and the adhesive as a dissolving, in case of the liquid flux the volume has increased in respective to the dry case suggesting that not the entire droplet volume has evaporated. In case of DI water the adhesive volume remained the same, however the roughness of the adhesive surface has increased, this issue was eliminated with slower rate of evaporation.

B. Bond Line Thickness and Die Tilt

The bond line thickness (BLT) is a key parameter affecting the mechanical reliability, electrical performance,

Authorized licensed use limited to: TU Delft Library. Downloaded on June 15,2026 at 10:18:25 UTC from IEEE Xplore. Restrictions apply.

and thermal resistance of an interconnect. Therefore, accurate BLT measurement is essential[14].

High-resolution 3D laser scans were used to obtain detailed surface profiles, from which the BLT was estimated by measuring the height difference between the mounted die and the corresponding PCB pad surface. The measurements were further verified using SEM imaging of cross-sections of the bond interface.

The significant BLT increase observed for acetone is mainly attributed to solvent penetration into the adhesive and bubble formation during drying and curing, resulting in a porous structure. A similar but less pronounced effect was observed for IPA. For DI water, the BLT increase may indicate incomplete evaporation or interaction with solvents originally present in the adhesive formulation. The increase in die tilt is primarily attributed to die shift during release onto the liquid droplet, which in some cases caused the die to move toward the edges of the adhesive layer where the thickness is slightly higher than in the central region.

Table 3 Average BLT of dies attached with different droplets after drying and full curing

Droplet	BLT after drying and curing (μm)
Dry	55.26±2.88
DI water	74.59±46
IPA	100.02±20
Acetone	147.11±4.91
Flux	88.38±5.44

Table 4 Maximum die tilt measured for die attached with different droplets

Droplet	Maximum Die tilt °
Dry	0.1
DI water	2.4
IPA	0.66
Acetone	3.97
Flux	1.47

C. Alignment

An important aspect of the bonding process is the final die position, or alignment accuracy, after placement. Non-reflowing materials such as adhesive pastes generally do not provide self-alignment, as they lack a transient liquid phase required for capillary self-alignment (CSA). In contrast, CSA is well established in solder reflow processes, where surface-tension-driven capillary forces can correct placement offsets when balanced with hydrodynamic drag.

In the dry experiments conducted in this study, dies were released from a small distance above a stencil-printed adhesive layer. Under these conditions, the final die position was determined mainly by the release process, the optical pre-alignment accuracy, and any initial placement offsets. Additional factors influencing placement include the die impact velocity, which depends on the release height and the air-puff pressure used for die detachment.

In droplet-assisted experiments, a confined droplet can enable die entrapment and potentially induce capillary self-alignment through surface tension forces. In the present experiments, acetone and IPA droplets were not confined and therefore did not exhibit self-alignment, whereas DI water and liquid flux droplets remained confined and enabled self-alignment. However, since die release was performed using a high-precision die bonder with accurate optical alignment and a short release distance, no significant die shift was observed. A more systematic study could be performed by intentionally introducing controlled lateral offsets to quantify the self-alignment capability.

V. Results

A. X-ray Inspection

X-ray imaging was performed using an offline X-ray inspection system (SEAMARK X5600) to evaluate the quality of die attachment. The inspection focused on assessing the interfacial contact between the dies and the adhesive, as well as identifying voids and interfacial discontinuities. As no external pressure was applied during assembly, limited wetting and partial interfacial contact were expected, which may result in locally reduced adhesive coverage and interfacial discontinuities that are commonly associated with reduced joint integrity. Image analysis was carried out using ImageJ software to quantify the effective contact area as a percentage of the total die area, providing a quantitative measure of adhesive coverage.

Table 5 Void area % of dies attached with different droplets

Droplet	Void area %
Dry	⩽3%
DI water	⩽12%
IPA	⩽17%
Acetone	~32%
Liquid Flux	ring-like void structure with diffuse contrast.

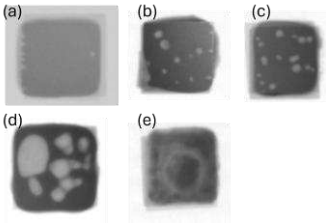


Fig. 6 X-ray images of 2mmx2mm dies (a) dry, (b) DI water, (c) IPA, (d) Acetone, and (e) Liquid flux.

B. Die-shear Strength

Die-shear strength measurements were carried out at room temperature using a Royce 650 Universal Bond Tester. The die-shear tool was positioned 100 µm above the substrate, and the tests were performed at a constant shear speed of 200 µm/s.[9]

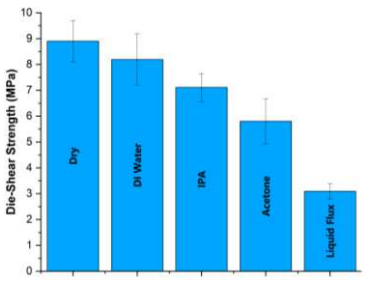


Fig. 7 Average die-shear strength of dies attached with different droplets.

Authorized licensed use limited to: TU Delft Library. Downloaded on June 15,2026 at 10:18:25 UTC from IEEE Xplore. Restrictions apply.

C. Bond Interface Microstructure

To examine the bond interfaces, samples were first mounted using KEM 20 cold-mounting resin, followed by grinding and polishing using a Qpol 300 M2 system from QATM. Microstructural examination and elemental analysis were carried out by scanning electron microscopy (SEM) combined with energy-dispersive X-ray spectroscopy (EDS). Inspections were performed using a Phenom XL G2 desktop SEM equipped with an EDS detector from Thermo Fisher Scientific.

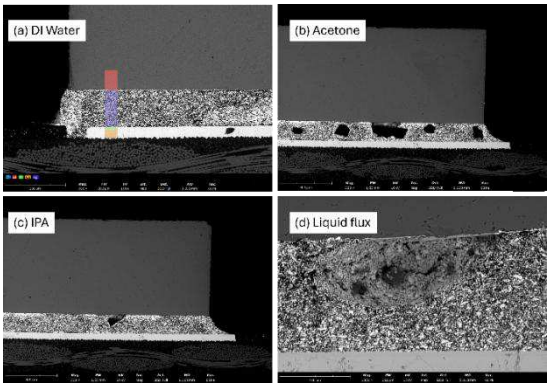


Fig. 8 SEM image of the bond interface of dies attached with different liquids (a) DI water, (b) Acetone, (c) IPA, (d) liquid flux.

D. Failure Analysis

Following the die-shear tests, a failure analysis was performed on both the PCB pad side and the die side to identify the failure modes and characterize the fracture surfaces. Initial optical inspection revealed adhesive residues on both surfaces, indicating a mixed failure mode with both adhesive and cohesive components. The fracture surfaces were further analyzed using high-resolution 3D surface topography measurements. A 3D laser scanning microscope was used to characterize the fracture morphology and quantify the surface topography.

Dies assembled using acetone exhibited a distinctive semi-spherical fracture morphology, suggesting the presence of gas bubbles trapped at the adhesive interface beneath the die. This defect is likely caused by acetone penetrating the adhesive layer and evaporating during drying, resulting in a porous interface structure. Upon fracture, these internal voids became visible, producing the observed morphology. A similar effect was observed for dies assembled using IPA, although with significantly lower severity.

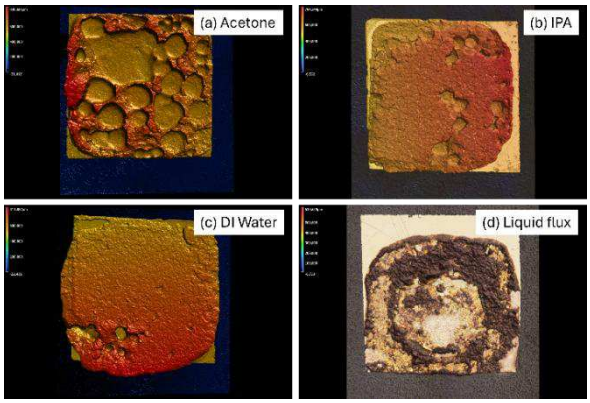


Fig. 9 3D scans of sheared dies which were attached with (a) Acetone, (b) IPA, (c) DI water, (d) Liquid flux.

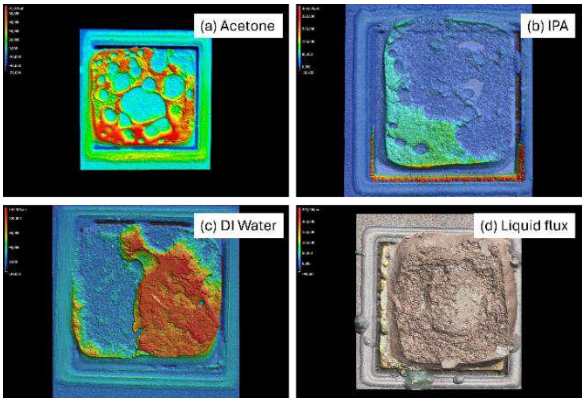


Fig. 10 3D scans of PCB bond pads after die-shear test of dies attached with (a)Acetone, (b)IPA, (c) DI water, (d)Liquid flux.

VI. Conclusion

This study investigates droplet-assisted microchip entrapment using experiments and two-dimensional simulations, focusing on the effect of droplet material properties while keeping the droplet volume, chip–substrate distance, and release position constant. The liquids considered include DI water, acetone, isopropyl alcohol (IPA), and liquid flux, which span a range of surface tension and viscosity values. The results show that surface tension controls the capillary forces responsible for chip stabilization, while viscosity governs the spreading rate, damping of oscillations, and the time required for the chip to reach equilibrium. Low-viscosity liquids such as acetone spread rapidly and lead to faster alignment, whereas higher-viscosity fluids such as liquid flux exhibit slower spreading and longer stabilization times. The simulations capture the key behaviors observed experimentally and provide insight into the transient fluid–structure interactions during chip entrapment. The results highlight the importance of selecting appropriate droplet materials to achieve reliable and controlled droplet-assisted micro assembly.

The combined simulation and experimental results further demonstrate that deionized (DI) water provides effective die entrapment and impact damping due to its relatively high surface tension, making it suitable for enabling contactless die attachment from a mechanical stabilization perspective. However, the presence of water negatively affected the resulting bond quality. In contrast, lower surface tension liquids such as IPA and acetone did not achieve full die entrapment under the tested conditions, mainly due to insufficient capillary confinement in the absence of physical confinement structures. Nevertheless, both liquids exhibited damping effects that enabled successful die transfer. Despite the expectation that these solvents would be more compatible with the bonding process, the experimental results showed bond quality limitations. In particular, acetone caused significant bubble formation within the adhesive layer during drying and curing, resulting in a porous structure, while IPA exhibited similar but less pronounced effects.

For liquid flux, the measured die shear strength was significantly lower and not acceptable, with failure occurring within the adhesive layer. This behavior suggests that the flux may have softened the adhesive or interfered

Authorized licensed use limited to: TU Delft Library. Downloaded on June 15,2026 at 10:18:25 UTC from IEEE Xplore. Restrictions apply.

with the curing process, potentially leading to incomplete curing. Further experiments with modified curing parameters, such as higher curing temperatures or longer curing times, may help determine whether incomplete curing is the primary cause of the reduced bond strength. In addition, replacing acetone and IPA with solvents that are chemically compatible with the adhesive formulation, as specified in the adhesive technical data sheet (TDS), may improve bonding performance. The relatively high solvent volumes used in the present experiments may also have contributed to defect formation.

Overall, the results indicate that an ideal liquid for droplet-assisted contactless die attachment should combine sufficiently high surface tension to ensure effective die confinement and stabilization with chemical compatibility with the adhesive system. The present study demonstrates that while water provides reliable die entrapment through strong capillary forces, bonding performance is strongly influenced by the interaction between the liquid and the adhesive. Consequently, liquids with tunable physical and chemical properties may offer a promising pathway for optimizing droplet-assisted die attachment. By carefully balancing surface tension, viscosity, and chemical compatibility with the adhesive, it may be possible to achieve improved die stabilization, controlled damping behavior, and robust bond formation.

ACKNOWLEDGEMENT

This work was funded by ITEC B.V. and co-financed by the Netherlands Enterprise Agency (RVO). The authors would like to thank the Else Kooi Laboratory (EKL), Kavli Nanolab Delft, and the Chip Integration Technology Centre (CITC) for their valuable support and contributions to this research.

REFERENCES

[1] H. E. Macaspac, J. F. Callanga, R. R. Dimagiba, and M. Mena, "Investigation of silicon die crack for varying silicon die parameters and die attach material," *Philippine Engineering Journal,* 2020.

[2] B. Majeed, I. Paul, K. M. Razeeb, J. Barton, and S. C. O'Mathuna, "Microstructural, mechanical, fractural and electrical characterization of thinned and singulated silicon test die," *Journal of Micromechanics and Microengineering,* vol. 16, no. 8, p. 1519, 2006/06/22 2006, doi: 10.1088/0960-1317/16/8/012.

[3] L. Ma and S. X. Bao, "Failure Analysis of Cracked Die," *ECS Transactions,* vol. 27, no. 1, p. 281, 2010/11/23 2010, doi: 10.1149/1.3360633.

[4] "A method for mounting an electronics component at a particular placement location on a carrier as well as a pick-and-place apparatus for mounting an electronics component at a particular placement location on a carrier," Patent WO2026017271A1 Patent Appl. Patent application, 2026. [Online]. Available: https://patentscope.wipo.int/search/en/WO2026017271

[5] V. Nassiet, B. Hassoune-Rhabbour, O. Tramis, and J.-A. Petit, "22 - Electrical and electronics," in *Adhesive Bonding (Second Edition)*, R. D. Adams Ed.: Woodhead Publishing, 2021, pp. 719-761.

[6] L. Riegger, O. Strohmeier, B. Faltin, R. Zengerle, and P. Koltay, "Adhesive bonding of microfluidic chips: influence of process parameters," *Journal of Micromechanics and Microengineering,* vol. 20, no. 8, p. 087003, 2010/07/12 2010, doi: 10.1088/0960-1317/20/8/087003.

[7] Y. Su, L. Zhang, B. Liao, Y. L. Mai, Y. Q. Dai, and W. Hu, "Simultaneous improvement of the electrical conductivity and mechanical properties via double-bond introduction in the electrically conductive adhesives," *Journal of Materials Science: Materials in Electronics,* vol. 31, no. 11, pp. 8923-8932, 2020/06/01 2020, doi: 10.1007/s10854-020-03427-2.

[8] U. Srinivasan, D. Liepmann, and R. T. Howe, "Microstructure to substrate self-assembly using capillary forces," *Journal of Microelectromechanical Systems,* vol. 10, no. 1, pp. 17-24, 2001, doi: 10.1109/84.911087.

[9] M. Park *et al.*, "Optimizing Binding Site Spacing in Fluidic Self-Assembly for Enhanced Microchip Integration Density," *Micromachines,* vol. 15, no. 3, p. 300, 2024. [Online]. Available: https://www.mdpi.com/2072-666X/15/3/300.

[10] C. J. Morris, S. A. Stauth, and B. A. Parviz, "Self-assembly for microscale and nanoscale packaging: steps toward self-packaging," *IEEE Transactions on Advanced Packaging,* vol. 28, no. 4, pp. 600-611, 2005, doi: 10.1109/TADVP.2005.858454.

[11] V. Dubey, J. Derakhshandeh, E. Beyne, J. P. Celis, and I. D. Wolf, "Fine Pitch Rapid Heat Self-Aligned Assembly and Liquid-Mediated Direct Bonding of Si Chips," *IEEE Transactions on Components, Packaging and Manufacturing Technology,* vol. 6, no. 6, pp. 946-953, 2016, doi: 10.1109/TCPMT.2016.2527793.

[12] I. White and M. J. Sully, "Macroscopic and microscopic capillary length and time scales from field infiltration," *Water Resources Research,* vol. 23, no. 8, pp. 1514-1522, 1987, doi: https://doi.org/10.1029/WR023i008p01514.

[13] G. Sekharan, J. Mohd Rohani, S. Yusof, and Z. Bakar, "Optimization Of Solder Paste Printing Parameters Using Design Of Experiments (DOE)," *Jurnal Teknologi,* vol. 43, 12/01 2005, doi: 10.11113/jt.v43.754.

[14] P.-C. Chen, C. Ming, L. Wei-Chung, and J. L. and Gabayno, "Bond line thickness and die tilt inspection in die bonding process," *Journal of the Chinese Institute of Engineers,* vol. 39, no. 4, pp. 508-512, 2016/05/18 2016, doi: 10.1080/02533839.2015.1125795.

Authorized licensed use limited to: TU Delft Library. Downloaded on June 15,2026 at 10:18:25 UTC from IEEE Xplore. Restrictions apply.